JOURNAL OF GEOPHYSICAL RESEARCH, VOL. 99, NO. C4, PAGES 7903–7916, APRIL 15, 1994

Eddy kinetic energy and momentum flux in the Southern Ocean: Comparison of a global eddy-resolving model with altimeter, drifter, and current-meter data

John L. Wilkin[1]
Antarctic Cooperative Research Centre, Hobart, Tasmania, Australia

Rosemary A. Morrow
Groupe de Recherche de Géodesie Spatiale, Toulouse, France

Abstract. The ability of a seasonally forced high-resolution global ocean general circulation model to simulate eddy variability and associated energy and momentum transfer processes in the Southern Ocean is assessed by comparing model statistics with observations. The observations include Geosat altimeter data analyzed for surface velocity variance at satellite ground track crossover points, current-meter data from the Agulhas and Campbell plateaus, and surface drifter data in the Tasman Sea. In western boundary currents and energetic regions of the Antarctic Circumpolar Current model eddy kinetic energy is lower than observed by typically a factor of 4, and in less energetic regions by a factor of 10. Differences in the location and extent of energetic regions are related to smoothness of the model bathymetry and other features of the model configuration. Eddy momentum flux divergence and eddy to mean kinetic energy conversion at the surface are diagnosed from the model. These show regions where eddy activity accelerates the mean flow through instability processes. Observational estimates of these terms are computed using mean flow gradients from hydrography climatology and altimeter eddy statistics. Several features of the spatial distribution of the observational estimates are consistent with the model and suggest that future calculations of mean currents from altimeter data will allow direct computation of eddy to mean current momentum and energy conversion terms.

1. Introduction

Ocean models are now being implemented with resolution sufficient to allow spontaneous generation of mesoscale eddies through instability processes. Examples are the Fine Resolution Antarctic Model [*FRAM Group*, 1991] of the Southern Ocean, the global model of *Semtner and Chervin* [1988, 1992], and the North Atlantic World Ocean Circulation Experiment (WOCE) model [*Bryan and Holland*, 1989; *Spall*, 1990; *Böning et al.*, 1991]. All are multilevel, primitive equation models that include realistic bathymetry, are driven with climatological wind and surface flux boundary conditions, and integrated long enough to calculate statistics of the mean and eddy fields. The models generally perform well at simulating the mean global circulation. They are less successful in reproducing the observed magnitude of mesoscale variability. For example, while the spatial distribution of mesoscale variability in the WOCE North Atlantic model agrees qualitatively with that observed by the Geosat altimeter, the magnitude of the surface height variability is too low by a factor of up to 4 in the central and, in particular, eastern Atlantic [*Stammer and Böning*, 1992]. Compared to current-meter measurements, the WOCE model eddy kinetic energy (EKE) is too low by a factor of 2 to 6 over a large depth range in the Canary Basin [*Spall*, 1990] and by more than a factor of 10 to 20 elsewhere in the eastern Atlantic [*Treguier*, 1992]. There are several reasons to expect low model eddy energy. The simulations were driven with monthly winds and therefore omit variability generated by weather-frequency wind forcing which may be significant, especially in the eastern Atlantic [*Treguier*, 1992]. Experiments varying the

[1] Also at CSIRO Division of Oceanography, Hobart, Tasmania, Australia.

Paper number 93JC03505.
0148-0227/94/93JC-03505$05.00

lateral friction coefficient show sensitivity of the EKE to subgrid-scale dissipation [*Böning et al.*, 1991]. But of greatest significance is model resolution. Energy and momentum exchange processes due to geostrophic turbulence occur on the horizontal scale of the first-mode Rossby radius. Consequently, autocorrelation length scales of surface height variability in the WOCE model and Geosat show a systematic decrease toward high latitudes as the Rossby radius decreases [*Stammer and Böning*, 1992]. However, the length scale decrease in the model is less pronounced than in the data and led *Stammer and Böning* [1992] to conclude that while the model resolution of 1/3° in latitude by 0.4° in longitude is adequate in the tropical and subtropical Atlantic, it is inadequate for resolving mesoscale variability poleward of 30°N. Doubling the resolution improved the simulation of eddy length scales poleward of 35°N [*Böning and Budich*, 1992] in an idealized basin version of the model. Decreased friction in the high-resolution case also contributed to increased EKE values throughout the model domain.

The present study examines mesoscale variability in the Southern Ocean in the global model of *Semtner and Chervin* [1988, 1992]. Southern Ocean observations from surface drifters [*Patterson*, 1985], current-meters [*Bryden*, 1983] and altimetry, all show high levels of eddy energy, particularly in the western boundary currents and major fronts of the Antarctic Circumpolar Current (ACC). *Bryden* [1983] emphasizes that the principal generation mechanism for this variability is baroclinic instability and that poleward eddy transport of heat is potentially important to the Southern Ocean heat balance. In quasi-geostrophic model studies, eddies also play a role in the Southern Ocean momentum balance. In these models, zonal momentum input by the wind is transferred meridionally by convergence of eddy momentum flux to intensify and concentrate the zonal jet that comprises the model ACC. By eddy form drag, momentum is transferred vertically to be balanced by topographic stress at the seafloor [*McWilliams et al.*, 1978; *Wolff et al.*, 1991]. Observational evidence for this process is provided by *Johnson and Bryden* [1989] who, by assuming eddy fluxes result primarily from baroclinic instability, related poleward eddy heat flux in the Drake Passage to the vertical flux of momentum and obtained a plausible balance for the ACC in this region.

The *Semtner and Chervin* [1988, 1992] model is described in section 2. Since the model resolution is comparable to the WOCE North Atlantic model, it is unlikely to be highly successful at simulating the magnitude and length scales of Southern Ocean mesoscale variability. Nevertheless, it should give a good description of the regional distribution of eddy variability, and it is instructive to examine where regional patterns observed by altimetry are modeled well and where they are not. Section 3 summarizes the analysis of Geosat data at ground track crossover points to resolve horizontal velocity variance and eddy momentum flux, or Reynolds stress. The current-meter and drifter data compared to the model are described in section 4. The comparison between modeled and observed EKE and eddy momentum flux is presented in section 5. Features of the energy and momentum balance are explored in section 6 and compared with similar terms computed from Geosat and Southern Ocean mean dynamic topography.

2. Description of the Model

The global ocean model analyzed here is described in detail by *Semtner and Chervin* [1988, 1992]. The model resolution is 0.5° latitude by 0.5° longitude, with 20 levels in the vertical. The model has been run in five stages of increasing realism. Throughout all stages, stability-dependent vertical mixing was used and surface fluxes were parameterized by restoring model surface temperature (T) and salinity (S) to observed climatology with a 30-day timescale. Stage 1 was a 10-year calculation where T and S were restored weakly (3-year timescale) at all depths to annual mean observed values, and annual mean wind forcing was applied. In stages 2 and 3 the restoring term was removed in the model thermocline (25- to 710-m depth) and lateral mixing decreased thereby allowing the quasi-steady circulation of stage 1 to spontaneously generate mesoscale variability through instability processes. Stage 4 incorporated seasonal winds and surface fluxes and was run for 10 years.

A fifth stage to the integration has since been completed. This was a rerun of the 10-year seasonal forced case but without the deep restoring to observed T and S. With deep restoring terms removed, regions of high eddy energy increased in extent although the maximum modeled values of EKE remained little changed. Since it is evident the restoring to observed T and S below 710-m depth damps mesoscale variability, eddy statistics from the tenth year of stage 5 are used in the comparison with observations. Here, the term "eddy" variability includes any departure of the instantaneous model solution from the mean for year 10. "Eddy" statistics computed in this manner therefore include a contribution from the seasonal cycle. However, this contribution is minor compared to the variability associated with the eddies and is consistent with the notion of "eddy" statistics commonly reported from the Geosat mission.

Surface velocity is computed from altimeter data by assuming geostrophic balance with the sea surface slope, whereas the model velocity also includes ageostrophic processes, notably, wind-driven Ekman flow. In the model, wind forcing is applied as a body force to the surfacemost level and vertical mixing is weak, so the Ekman flow is largely contained within level 1. The model velocities used in the comparison with altimeter geostrophic velocities are therefore taken from level 2 of the model centered at 32.5-m depth.

3. Geosat Data Analysis

The analysis of Geosat altimeter data used here is described in detail by *Morrow et al.* [1992, 1994]. Two years of data were used to compute components of sur-

face geostrophic velocity at crossover points of the satellite ground track. Uncertainty in the geoid makes accurate calculation of the absolute velocity impossible at present. However, the time variable (or eddy) component of velocity is readily obtained once standard corrections for atmosphere and orbit errors are applied and the mean sea surface height is removed. The ground track velocity components were interpolated to a common time and rotated to east and north components (u', v'). From these eddy velocity time series ensemble average EKE and eddy momentum flux were computed for 2° latitude by 2° longitude bins.

Equatorward of 30° latitude the satellite ground tracks are not sufficiently orthogonal to allow reliable separation of the two velocity components. Furthermore, in the equatorial Atlantic, systematic differences were found between eddy length scales from Geosat and the WOCE model [*Stammer and Böning*, 1992] despite the relatively high resolution of the model compared to the Rossby radius at low latitudes. This was attributed to a bias introduced by the poor signal to noise ratio of altimeter data in the tropics. For these reasons only data from south of 30°S are considered in the present study.

4. Other Data: Drifters and Current-meters

Drifter data are available for comparison with the model from a 30-year surface drifter program in the Tasman Sea. Velocity variance estimates from these data have been averaged in 1° latitude by 1° longitude bins (G. R. Cresswell and J. L. Peterson, Satellite drifter measurements of current energies in the Tasman Sea, unpublished manuscript, 1993). This resolution is comparable to Geosat and provides an alternate view of eddy variabilty in a western boundary current system, namely, the East Australian Current. Some of the differences between drifter and altimeter data can be explored by extending the comparison to model results.

A comparison of subsurface observations of currents in the Southern Ocean with the model will be presented using data from two long-term current-meter deployments. Seventeen months of data are available from a mooring deployed southeast of New Zealand at 49.4°S, 189.5°E [*Bryden and Heath*, 1985]. Instruments ranged in depth from 1000 m to 5000 m below the surface. Also, 2 years of current measurements were made in the Agulhas region at five mooring sites with instruments deployed at depths ranging from 200 m below the surface to the seafloor [*Luyten et al.*, 1990].

5. Comparison of Model and Observations

5.1. Eddy Kinetic Energy

Eddy kinetic energy in the Southern Ocean from Geosat is compared to the model in Plate 1. The most energetic regions coincide, namely, the axis of the ACC (in particular over the Southeast Indian Ridge), the Agulhas Current, the East Australian Current separation, and the Brazil–Malvinas Current confluence. However, throughout most of the Southern Ocean, model eddy energy is much lower than Geosat (Plate 2). Between 30°S and 60°S the mean model EKE is 6.20×10^{-3} $m^2\ s^{-2}$, the mean Geosat EKE is 1.59×10^{-2} $m^2\ s^{-2}$, and the mean ratio is 0.17 or roughly 1:6. The pattern of this ratio is similar to the EKE distribution itself, being generally smaller away from energetic regions. Where observed EKE is greater than 2.0×10^{-2} $m^2\ s^{-2}$ (24% of the area), the mean ratio is 1:4.4. Where the model is less energetic than 5.0×10^{-3} $m^2\ s^{-2}$ (86% of the area), the mean ratio is 1:12.3. Table 1 shows zonal averages in 2° latitude bands for these energy regimes. For energetic regions between 40°S and 45°S the ratio is between 1:2.2 and 1:4. Outside this latitude range the model performance relative to Geosat is poorer.

In low-energy regions and at low latitudes, Geosat altimeter measurement errors can adversely affect EKE estimates [*Morrow et al.*, 1994]. Furthermore, in the subtropics there may be a significant contribution to eddy variability from weather-frequency forcing, a process not included in the model. For these reasons, low model EKE values compared to Geosat in low-latitude and relatively quiet regions do not necessarily indicate a serious deficiency in the model. Nevertheless, it is clear the model underestimates EKE by typically a factor of at least 4.

This factor of 4 in EKE is consistent with previous comparisons based on sea surface height variability [*Semtner and Chervin*, 1992] and with results from the comparable resolution WOCE North Atlantic model [*Stammer and Böning*, 1992]. The baroclinic instability process that converts large-scale potential energy to eddy-scale potential and kinetic energy occurs on the length scale of the first-mode Rossby radius. *Stammer and Böning* [1992] found the resolution of the WOCE North Atlantic model was inadequate for simulating eddy length scales north of 30°N because of model resolution relative to the Rossby radius. Rossby radii in the Atlantic Ocean compared to resolution of the WOCE and Semtner and Chervin (SC) models are shown in Table 2. At 30°N the WOCE model resolution is close to one Rossby radius. In the South Atlantic the SC model achieves this resolution between 20°S to 30°S. Therefore it is expected that in the Southern Ocean the SC model is only marginally eddy-resolving and will not match the observed magnitude of eddy variability, especially at high latitudes.

Differences are not only due to model resolution at high latitudes or Geosat error at low latitudes. There are also distinct regional differences. Regions of high energy are evident in the data but absent from the model (Plate 1), namely, the Agulhas Basin (30°E, 50°S), downstream from Kerguelen Plateau at 90°E, the Leeuwin Current in southwest Australia, Macquarie Ridge and the Campbell Plateau (150°E to 170°E), the mid-Pacific Ridge, the Scotia Sea, and the Malvinas Current. These discrepancies are considered in sections 5.3 and 7.

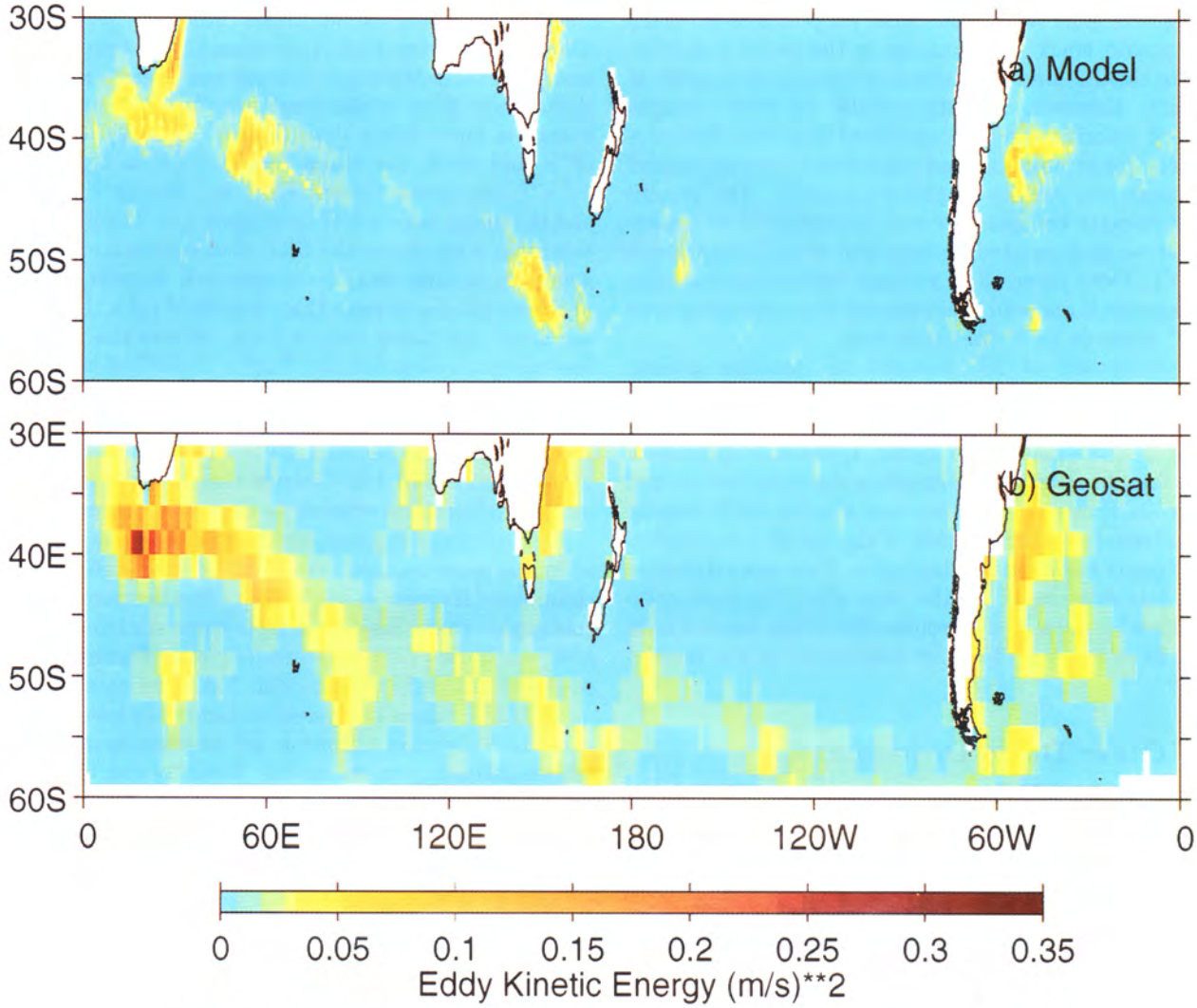

Plate 1. Eddy kinetic energy (EKE) in the Southern Ocean: (a) model and (b) Geosat.

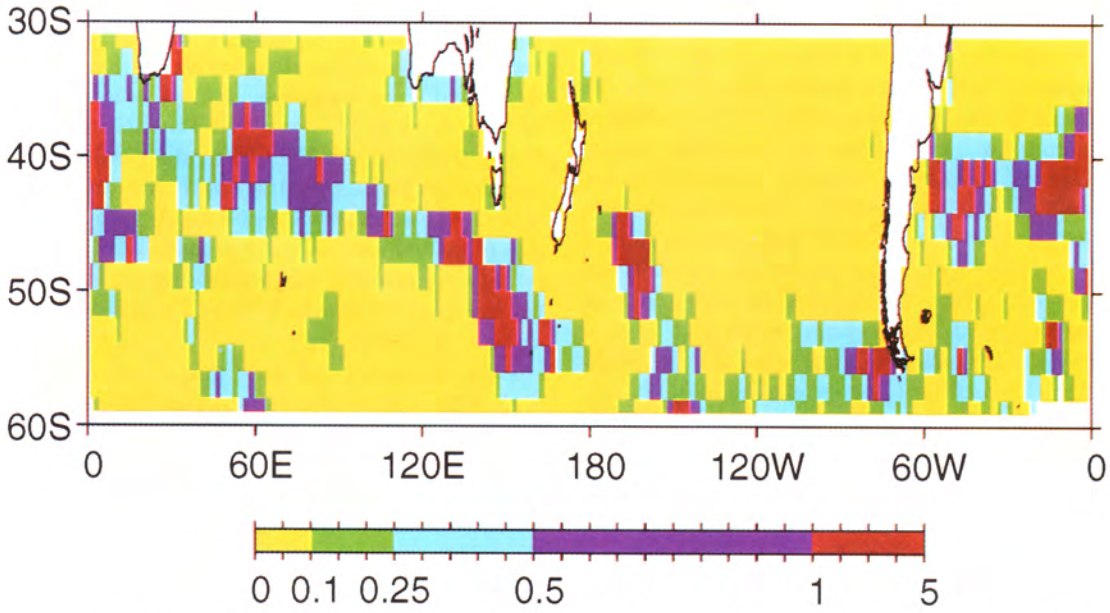

Plate 2. Ratio of EKE from the model to Geosat in the Southern Ocean. The 0.5° resolution model results are averaged to 2° bins prior to computing the ratio.

5.2. Eddy Momentum Flux and Velocity Variance Ellipses

High-resolution quasi-geostrophic model studies indicate that in the Southern Ocean, eddies play a role in the zonally integrated momentum balance by transferring zonal momentum meridionally through convergence of the $\overline{u'v'}$ component of the eddy momentum flux [*Wolff et al.*, 1991]. The momentum of the narrow zonal jet is subsequently balanced by other processes. The pattern of $\overline{u'v'}$ computed by *Morrow et al.* [1992] from Geosat supports this result by showing a tendency for regions of negative $\overline{u'v'}$ to occur to the north of zonal mean flows and positive $\overline{u'v'}$ to the south. A similar tendency is found in the model, but as was the case for EKE, model $\overline{u'v'}$ is lower than observed by typically a factor of 4.

Table 1. Zonal Mean Ratio of Geosat EKE to Model EKE by Latitude

	Geosat EKE/Model EKE		
Latitude	All Bins	Geosat EKE $\geq$ 0.02 m^2s^{-2}	Model EKE $\leq$ 0.005 m^2s^{-2}
-31	14.7	5.1	24.5
-33	10.2	2.7	23.1
-35	7.4	3.1	11.9
-37	7.3	5.2	16.9
-39	3.6	2.4	14.4
-41	3.0	2.3	9.5
-43	3.1	2.5	9.3
-45	3.8	4.0	5.5
-47	3.4	9.1	8.7
-49	6.0	10.8	13.3
-51	5.9	2.4	15.2
-53	5.3	3.2	9.3
-55	4.8	2.9	8.5
-57	6.3	7.8	7.5
-59	6.9	9.5	7.1

EKE, eddy kinetic energy. Column 2, mean over all ocean bins. Column 3, mean for energetic regions where Geosat EKE $\geq$ 0.02 m^2 s^{-2}. Column 4, mean for relatively quiet regions where model EKE $\leq$ 0.005 m^2 s^{-2}.

However, locally, the $\overline{u'v'}$ term alone does not indicate the sense of eddy momentum flux work on the mean flow except where the mean flow is strictly zonal. This requires computation of the divergence of all components of the eddy momentum flux and is presented in section 6. However, the sense of eddy work on the mean flow can be examined qualitatively by considering velocity variance ellipses computed from the three components of the horizontal eddy momentum flux: $\overline{u'^2}$, $\overline{v'^2}$, and $\overline{u'v'}$. Anisotropic eddy fluctuations are represented by an elongated ellipse, with the principal direction of the velocity variance aligned with the major axis of the ellipse. Ellipses with major axis in the northeast (southeast) quadrant indicate eastward velocity perturbations are correlated with northward (southward) velocity perturbations. Local eddy momentum flux convergence is thus likely in a frontal region where the major axes of surrounding velocity variance ellipses point obliquely toward the front but in the direction of the local mean flow.

For example, over the Southeast Indian Ridge near 150°E the ACC flow is toward the southeast and large velocity variance ellipses indicate substantial eddy energy (Plate 3). To the north of the mean current, variance ellipses point slightly south-southeast, while to the

Table 2. Rossby Radii (Ro) Relative to Model Resolution for the Semtner and Chervin (SC) model and the WOCE North Atlantic model

		SC Model (Δy = 55.6 km)			WOCE Model (Δy = 37.0 km)		
Latitude	Ro, km	Δx, km	Ro/Δx	Ro/Δy	Δx, km	Ro/Δx	Ro/Δy
60	7	27.8	0.25	0.13	22.2	0.32	0.19
50	12	35.7	0.34	0.22	28.6	0.42	0.32
40	20	42.6	0.47	0.36	34.0	0.59	0.54
30	35	48.1	0.73	0.63	38.5	0.91	0.95
20	50	52.2	0.96	0.90	41.8	1.20	1.35
10	100	54.7	1.83	1.80	43.8	2.28	2.70
0	350	55.6	6.30	6.30	44.4	7.88	9.45
-10	100	54.7	1.83	1.80	43.8	2.28	2.70
-20	55	52.2	1.05	0.99			
-30	35	48.1	0.73	0.63			
-40	23	42.6	0.54	0.41			
-50	13	35.7	0.36	0.23			
-60	6	27.8	0.22	0.11			
-70	5	19.0	0.26	0.09			

WOCE, World Ocean Circulation Experiment. Ro values for the North Atlantic are from *Emery et al.* [1984] and South Atlantic from *Houry et al.* [1987].

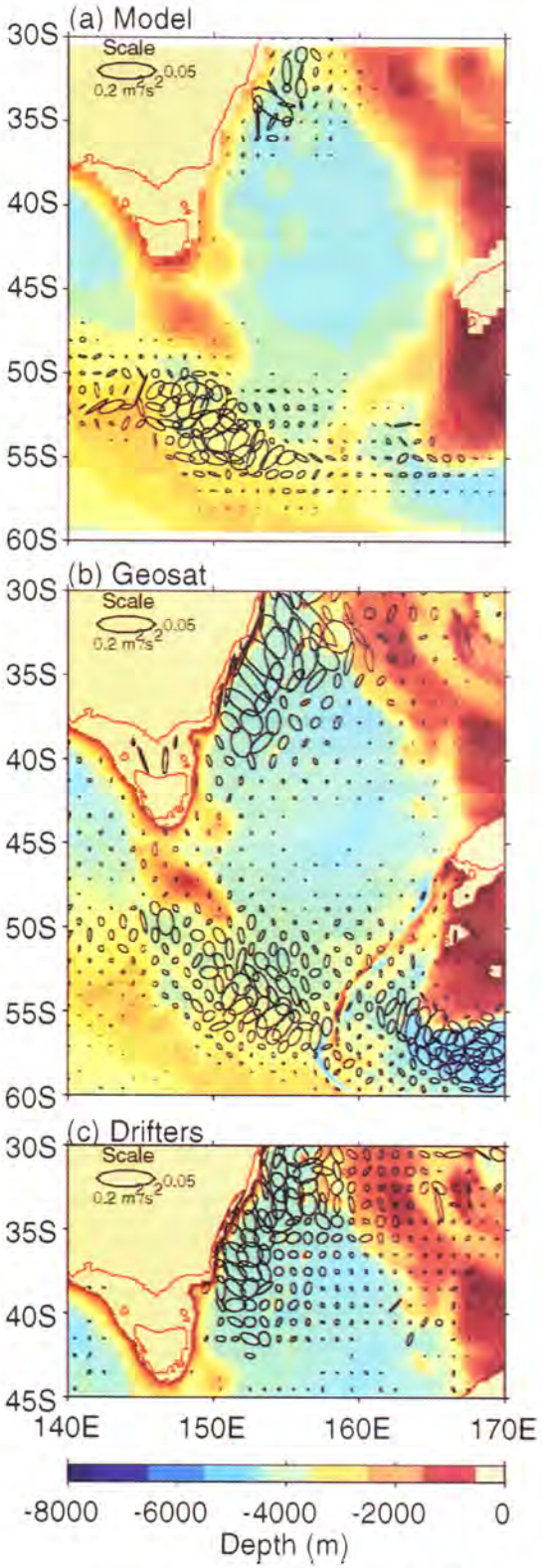

Plate 3. Velocity variance ellipses in the Tasman Sea and adjacent sector of the Southern Ocean. Scale ellipse has semimajor axis of 0.2 $m^2\ s^{-2}$ and semiminor axis of 0.05 $m^2\ s^{-2}$. (a) Model results plotted over model bathymetry. (b) Geosat observations at crossover points and (c) long-term surface drifter observations plotted over true bathymetry.

south of the ACC they point slightly east-southeast, indicating eddy momentum convergence toward the ACC axis in this region. As *Wolff et al.* [1991] noted, this anisotropy results from eddies being "tilted" by the reduction of the local Rossby wave phase speed by the mean flow. Similar features can be observed in other regions and are discussed in the next section.

The result that the eddy field has significant regions of anisotropy is a caution against basing altimeter estimates of eddy energy solely on variability in the along-track component of surface slope.

5.3. Regional Comparisons

Macquarie Ridge. The Macquarie Ridge at 160°E, 47°–55°S, is one of the major topographic barriers impeding the ACC. After crossing the Macquarie Ridge, the model ACC is forced south of the Campbell Plateau at 170°E then turns north following f/h contours [*Semtner and Chervin,* 1992, Plate 5 and Figure 14]. Velocity variance ellipses for this region computed from Geosat, the model, and surface drifters are compared in Plate 3.

Drifters and Geosat (Plates 3b and 3c) show the deep basin south of Campbell Plateau is a region of high eddy energy, yet the model (Plate 3a) shows little enhanced eddy energy in this region. There is however, a highly energetic region immediately upstream on the northern flank of the Southeast Indian Ridge where the model EKE maximum of 0.134 $m^2\ s^{-2}$ at 53°S, 150°E actually exceeds the Geosat local maximum of 0.05 $m^2\ s^{-2}$. The weak model EKE downstream from Macquarie Ridge is likely to be the result of the model bathymetry being overly smooth in this region. The Macquarie Ridge appears in Plate 3b as a red streak extending southwest from New Zealand. Comparison with Plate 3a shows the smoothing applied to the model bathymetry [see *Semtner and Chervin,* 1988] has virtually eliminated the very steep short horizontal scale bathymetric features that comprise Macquarie Ridge and also affected, but less severely, the escarpment at the edge of Campbell Plateau.

Upstream of 145°E the model ACC is a narrow jet steered by the bathymetry of the Southeast Indian Ridge [*Semtner and Chervin,* 1992, Figure 14]. Crossing 145°E, the jet enters a relatively uniform depth basin where there is little bathymetric control of the flow and the jet subsequently breaks up into transient eddies. Animations of model output [*Isakari et al.*, 1992] show clearly the transition from a jet to vigorous eddy activity and that the model eddies dissipate rapidly. There is no obvious ACC jet between 150°E and 165°E, and no model Macquarie Ridge to contribute to intensification or instability of a mean current, thereby accounting for low eddy energy around 160°E. East of 165°E the model ACC reestablishes itself as a narrow current following closely the smoothed bathymetry of Campbell Plateau. It is a strong but stable mean current that meanders little and sheds no eddies, thus model EKE is again low around the Campbell Plateau.

Tasman Sea and East Australian Current. The western boundary current of the South Pacific, the East Australian Current (EAC), flows south along the Australian coast but separates near 32°S to form the Tasman front. In the region 30°S to 40°S, 140°E to 170°E, the mean model EKE is 0.0049 m^2 s^{-2} which is substantially less than that from Geosat (0.0417 m^2 s^{-2}) and surface drifters (0.0341 m^2 s^{-2}). In Plate 3, Geosat and drifter data show that a region of high eddy variability extends from the coast to Lord Howe Rise (160°E), whereas the model EKE is trapped much closer to the coast. Thus though the mean transport of the EAC is simulated quite well [*Semtner and Chervin*, 1992], the model EAC fails to exhibit the level of instability and hence eddy energy expected from observations, and the model eddies dissipate too rapidly.

Although the magnitude and eastward extent of the model EKE are too small, the pattern of velocity variance shows reasonable qualitative agreement. The variance ellipses are oriented alongshore near the coast in the model, as they are in observations. Immediately offshore, the ellipse principal axes are oriented southeast-northwest and turn to northeast-southwest farther offshore. This turning is associated with the first meander of the Tasman front which generally occurs between 152°E and 156°E [*Mulhearn*, 1987] and is captured in the model mean flow [*Semtner and Chervin*, 1992]. Near 33°S, 157°E, model variance ellipses are oriented strongly north-south consistent with a Tasman front that varies meridionally in position but maintains a steady zonal transport. This behavior is evident in animations of the model output [*Isakari et al.*, 1992]. However, observed variance ellipses are more isotropic in this region, indicating the Tasman front is more variable in position and strength.

A further difference between model and observations is seen immediately adjacent to the Australian coast where the model energy is low but Geosat, and to a slightly lesser extent the drifters, show appreciable eddy energy. This is most likely the result of the model no-slip boundary condition and the staircase discretization of the coastline, both contributing to weak currents in the model boundary layer.

Morrow [1994] compared Geosat and drifter observations in this region in detail, concluding that Geosat variance ellipses tend to be less isotropic than drifter ellipses and show sharper spatial gradients between regions of high and low eddy energy. These features were attributed to the additional spatial averaging inherent in drifter observations and that drifter data include high-frequency wind-driven ageostrophic currents which may cause drifter EKE to be greater than Geosat in relatively quiescent regions. The model EKE values are more akin to Geosat observations than drifter observations, being computed as the average over time of velocities at fixed locations. The result that the model variance ellipses are less isotropic than the drifter ellipses and more spatially variable in magnitude supports *Morrow's et al.* [1994] conjecture.

Agulhas Current. Model and Geosat EKE for the Agulhas Current region is shown in Plates 4b and 4c. A local maximum in both EKE distibutions occurs near 40°S, 20°E, and high values extend eastward from this point. These energetic regions are associated with meandering of the Agulhas retroflection and eddies shed by the current. However, as noted in section 5.1, model EKE is consistently weaker than observed, and there are significant local differences in the EKE patterns. Observed EKE is high throughout the Agulhas return current (35°E to 65°E) due to meandering of the mean current position, whereas model EKE is very low between 35°E and 45°E. The model mean flow is almost uniformly zonal in this region until it crosses the Southwest Indian Ridge at 47°E and takes several large meanders (Plate 4a). East of the ridge crest, model EKE increases markedly (Plate 4b). It appears therefore that meandering of the model mean current triggered by instabilities in the Agulhas Plateau region is damped rapidly and the mean current subsequently becomes steady and zonal until it reaches the Southwest Indian Ridge. Here, interaction with bathymetry triggers further variability in the current and accounts for the increased EKE from 50°E to 65°E.

The model results shown here from stage 5 of the integration differ noticeably in the Agulhas region from those of stage 4 which included deep restoring to climatology. In the stage 4 results (not shown) there are two local maxima in EKE, at 37°S, 17°E, and 40°S, 30°E, separated by relatively low EKE of 0.02 m^2 s^{-2} where the local maximum occurs in the stage 5 results and Geosat. Thus the deep restoring to climatological T and S below 710-m depth, albeit with a long 3-year timescale, has a significant impact on the tendency of the model Agulhas Current to meander and generate long-lived eddies.

Observations from current-meter moorings in the Agulhas region [*Luyten et al.*, 1990] provide a comparison with the depth structure of the model EKE (Figures 1a–1e). The ratio of modeled to observed EKE is approximately uniform throughout the water column at all sites, indicating the model captures the vertical structure of eddy energy quite well. Model vertical resolution is adequate for resolving at least the first baroclinic mode. Therefore a reasonable simulation of the vertical structure of eddy energy is expected if the eddy variability is dominated by the barotropic and first baroclinic modes, as it is elsewhere in the Southern Ocean [*Inoue*, 1985]. The model EKE near the site of the *Bryden and Heath* [1985] mooring is extremely low at all depths (Figure 1f). As noted earlier, the model ACC in this region flows steadily along the flank of the Campbell Plateau exhibiting little variability. The current-meter data and Geosat, which are in reasonable agreement, highlight the Campbell Plateau region of the model as providing a particularly poor simulation of eddy variability.

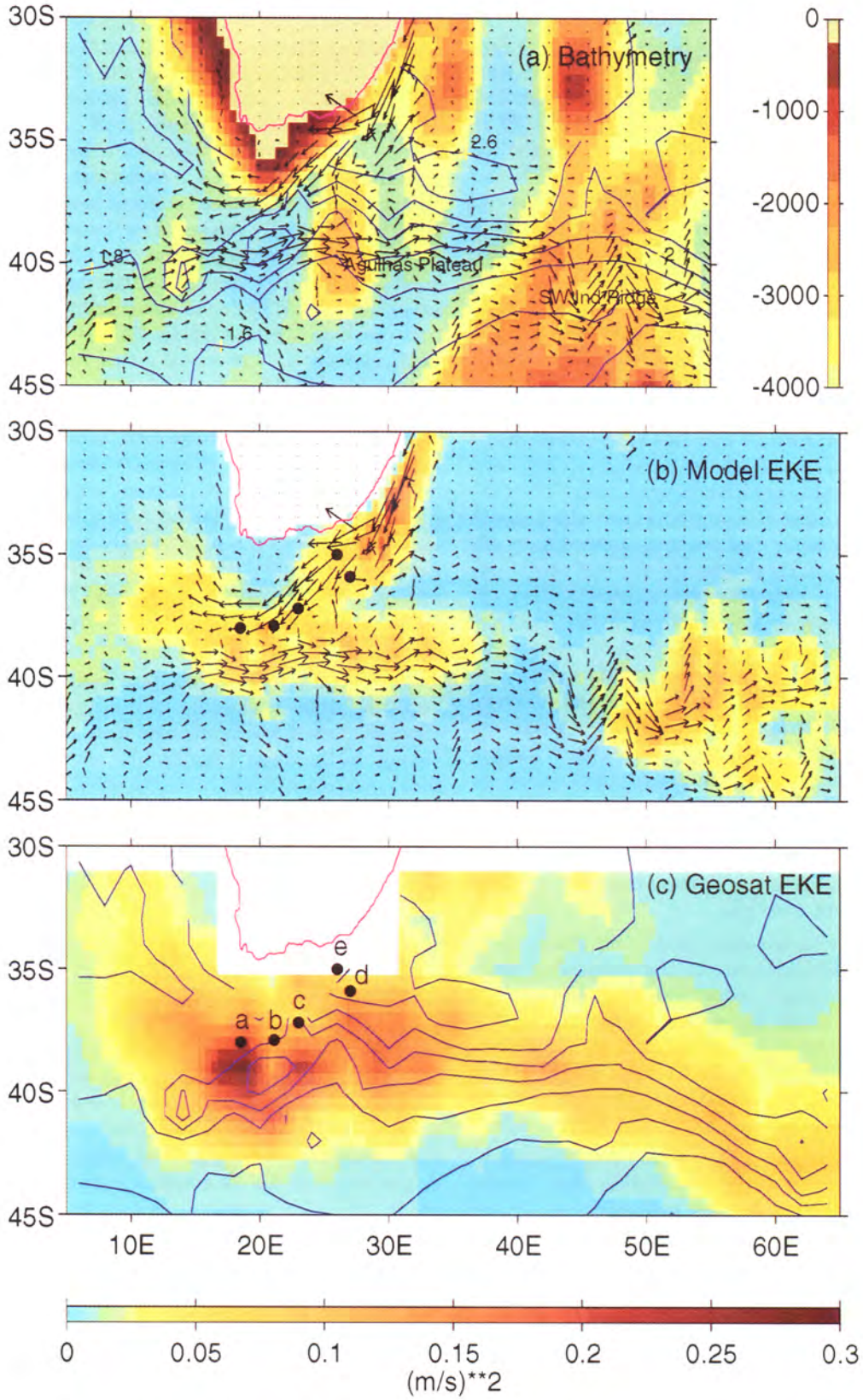

Plate 4. Eddy kinetic energy and mean currents in the Agulhas Current region. (a) Model bathymetry, model mean velocity vectors, and observed mean dynamic topography (contour interval 0.2 dynamic meters) from *Gordon and Molinelli* [1982]. EKE for (b) model and (c) for Geosat. Solid circles show the location of the moorings referred to in the text and Figures 1a–1e.

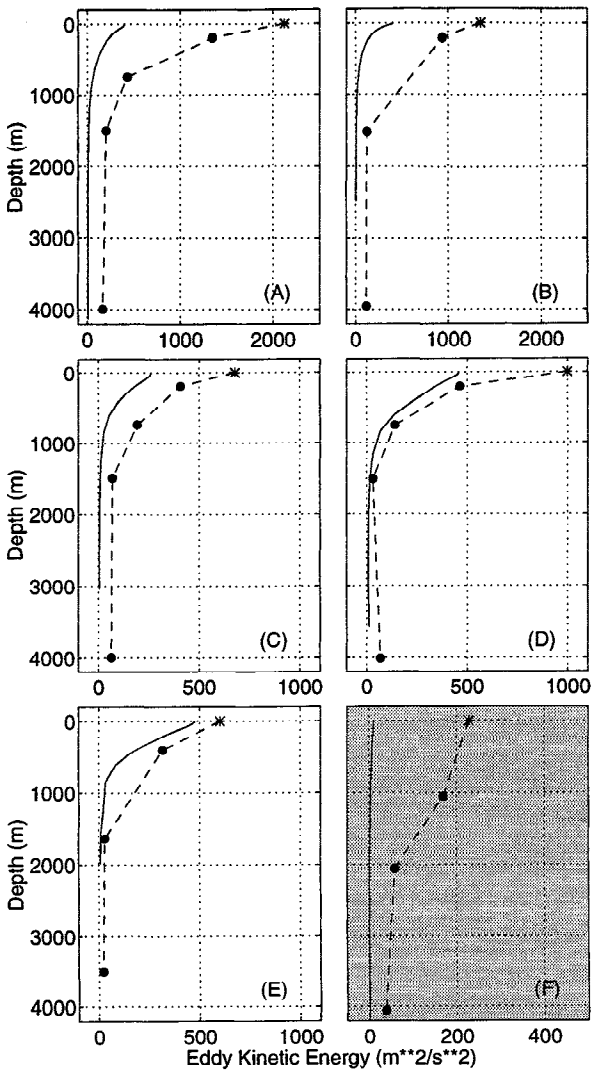

Figure 1. Eddy kinetic energy ($m^2\ s^{-2}$) from the model (solid line) compared to surface values from Geosat (asterisk) and long-term current-meter records (solid circle). Geosat values are bilinearly interpolated to the mooring location from the four closest crossover points. Dashed line links observations. (a–e) Mooring sites in the Agulhas region [*Luyten et al.*, 1990]. (f) Current-meter data from the Ridge Array (49°40'S, 170°30'W) southeast of New Zealand [*Bryden and Heath*, 1985].

6. Eddy-Mean Flow Interaction

Eddy-mean flow interaction processes, such as convergence of eddy momentum flux accelerating the mean current and EKE generation through barotropic and baroclinic instabilities, cannot presently be examined with altimeter data alone because the marine geoid is not known with sufficient accuracy to give reliable estimates of mean geostrophic currents. However, such calculations can be attempted by estimating mean currents from hydrography and combining these with eddy statistics from Geosat. Here, mean currents are computed from the gradient of surface dynamic height relative to 2000 db from the 1° latitude by 2° longitude gridded values of *Gordon and Mollineli* [1982]. Where the ocean is shallower than 2000 m, mean currents and eddy-mean flow interactions are not computed. To see if the result is plausible, the outcome is compared with momentum and energy conversion terms computed from the model, which provides a self-consistent set of mean current and eddy statistics.

6.1. Kinetic Energy Conversion

The conversion of EKE to mean kinetic energy (MKE) is given by (see Appendix)

$$\overline{u'u'}\frac{\partial \overline{u}}{\partial x} + \overline{v'u'}\frac{\partial \overline{v}}{\partial x} + \overline{u'v'}\frac{\partial \overline{u}}{\partial y} + \overline{v'v'}\frac{\partial \overline{v}}{\partial y}$$

Where this term is positive, EKE is being converted to MKE at that location through the Reynolds stresses doing work on the mean shear so as to accelerate the mean flow.

Focusing on the Agulhas Current region, where eddy energy is greatest in the data and model, Plate 5 compares EKE to MKE conversion rates from hydrography and Geosat to the model. There are several points of qualitative agreement. An area of significant EKE to MKE conversion (red) occurs west of the Agulhas Plateau near 20°E, 40°S. Immediately east of this region the model shows MKE to EKE conversion (blue) on the western flank of the Agulhas Plateau. The data show the same sense to energy conversion in this region but of weaker magnitude. Still farther east, in the region 27°E to 30°E, model and data show EKE to MKE conversion. This area includes the top of the Agulhas Plateau and its western flank. The data show EKE to MKE conversion atop the Southwest Indian Ridge (49°E), whereas the model suggests this process occurs downstream from the ridge. The region of MKE to EKE conversion at 16°E, 38°S in the model occurs where the Agulhas Current retroflects and begins to flow eastward and the model regularly generates eddies that move west into the Atlantic [*Isakari et al.*, 1992]. The data show the same sense to energy conversion here but it is extremely weak and displaced slightly south as is the retroflection point itself. Another region of active eddy generation in the model is the western boundary current prior to its separation from the coast. It is not possible to examine the corresponding region in the data because the gridded hydrographic climatology is too coarse to capture the western boundary current, and Geosat data have not been considered in bins that cross the coast. However, where the negative energy conversion region in the western boundary current extends offshore near 28°E, 36°S in the model, there is a corresponding region in the data.

Forcing by wind stress, τ, contributes approximately $(\tau/\rho)\times$(mean current)/(Ekman layer depth) = (0.1 Pa/10^3 kg m^{-3})(0.5 m s^{-1})/(50 m) = $1\times10^{-6} m^2\ s^{-3}$ to the mean kinetic energy balance, which is comparable to the estimated kinetic energy conversion rate of $\pm4\times10^{-7} m^2\ s^{-3}$ in this region.

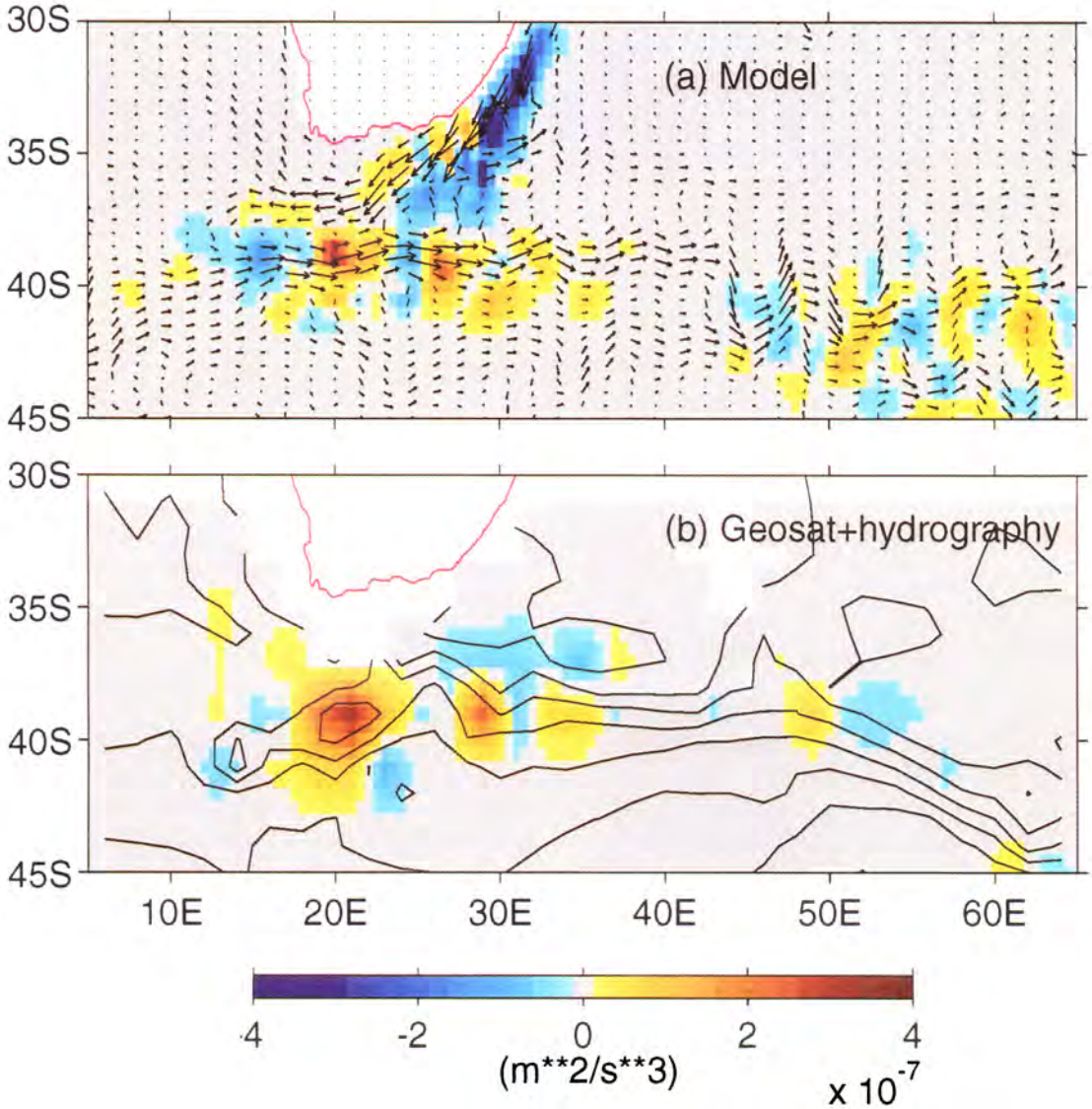

Plate 5. Rate of transfer of kinetic energy of eddies to kinetic energy of the mean flow in units $m^2\ s^{-3}$. (a) Model. (b) Observational estimate using Geosat eddy statistics and *Gordon and Molinelli* [1982] mean dynamic topography. Positive indicates the mean flow is drawing energy from the eddies. Respective mean currents are indicated by model mean vectors and observed dynamic topography, as in Plate 4.

6.2. Eddy Momentum Flux Divergence

When the divergence of horizontal eddy momentum flux in the local alongstream direction,

$$-\frac{\overline{u}}{|\overline{\mathbf{u}}|}\left(\frac{\partial}{\partial x}\overline{u'u'}+\frac{\partial}{\partial y}\overline{v'u'}\right)-\frac{\overline{v}}{|\overline{\mathbf{u}}|}\left(\frac{\partial}{\partial x}\overline{u'v'}+\frac{\partial}{\partial y}\overline{v'v'}\right)$$

is positive (see Appendix), eddies locally accelerate the momentum of the mean current. Plate 6 compares this term computed from hydrography and Geosat to the model for the Agulhas region.

In the observations, positive eddy momentum flux divergence (red/yellow) tends to coincide with the axis of the Agulhas return current which roughly follows the two-dynamic meter contour. These regions are generally flanked by negative eddy momentum flux divergence (blue), a pattern consistent with quasi-geostrophic channel models of zonal currents. In the model the strongest positive regions also coincide with the model return current from 20°E to 35°E. West of 20°E there is little agreement between model and observations. The modeled area of negative divergence at 16°E, 39°S coincides with negative energy conversion in Plate 5. The observations show no such correspondence. This may betray shortcomings in the observational estimates due to the combination of altimeter and hydrography data from nonoverlapping time periods, or simply indicate that dynamical processes other than barotropic instability or Reynolds stress divergence are more important.

Estimating the magnitude of momentum input by wind as $(\tau/\rho)/(\text{Ekman depth}) = (0.1\ \text{Pa}/10^3\ \text{kg m}^{-3})\ /\ (50\ \text{m}) = 2\times10^{-6}\text{m s}^{-2}$ it is apparent that eddy momen-

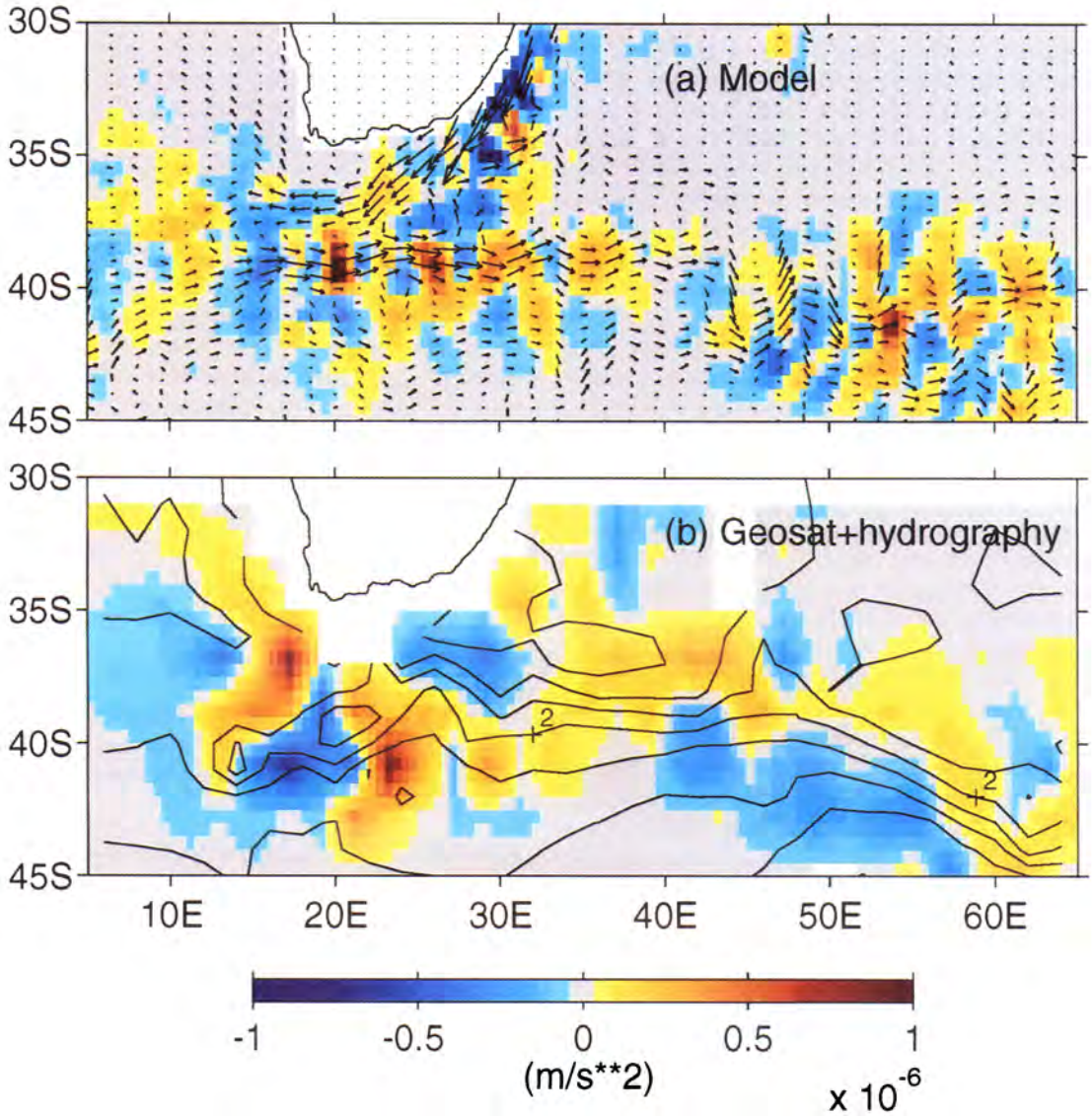

Plate 6. Eddy momentum flux divergence in local alongstream coordinates in units m s^{-2}. (a) Model. (b) Observational estimate using Geosat eddy statistics and mean dynamic topography. Positive indicates that the divergence of eddy momentum flux accelerates the local mean current. Respective mean currents are indicated by model mean vectors and observed dynamic topography, as in Plate 4.

tum flux divergence of $\pm 1 \times 10^{-6}$m s^{-2} in this region is significant in the regional momentum balance.

Thus within isolated regions such as the Agulhas Current, eddy-mean flow interaction processes appear to be significant in the kinetic energy and momentum balances even at the marginal resolution of the model and data examined here.

7. Discussion and Summary

Throughout the Southern Ocean the geographic distribution of eddy variability simulated in the model agrees well with that observed by the Geosat altimeter. However, where eddy variability is high, along the axis of the ACC and in western boundary currents, the model underestimates EKE by typically a factor of 4. Other models of comparable resolution (e.g., the WOCE North Atlantic model) exhibit similar performance, and this is recognized as being the result of low model resolution relative to the first-mode Rossby radius, particularly at high latitudes. Where eddy variability is low, the model underestimates EKE by typically a factor of 10, even at low latitudes. This is attributed to Geosat instrument noise giving erroneously high eddy energy, and the absence from the model of high weather-frequency wind forcing. In addition to these overall differences in eddy energy, there are several regional discrepancies.

In the Macquarie Ridge region the model bathymetry lacks several short horizontal scale features, principally seamounts. Low model EKE in this region is likely the result of the smoothed bathymetry failing to trigger in-

stability in the mean current. Other regions where the true bathymetry is steep and highly variable but this detail is lost in the model are the Agulhas Basin (30°E, 50°S), downstream from the Kerguelen Plateau at 90°E, where the ACC crosses the mid-Pacific Ridge at 140°W, and the Scotia Sea. All are regions where model EKE is lower than expected compared to Geosat. Regions where the model mean currents are steered strongly by bathymetry include the EAC and along the east side of Campbell Plateau. These boundary currents exhibit little variability and, consequently, much lower EKE than observed. The smooth and continuous f/h contours of the model may lead to overly stable mean currents in these and other boundary current regions with lower than observed EKE, namely, the Leeuwin and Malvinas Currents. Accurate representation of bathymetric detail therefore appears to be important to the simulation of Southern Ocean EKE distribution. Experiments with a similar resolution model modified to eliminate the need for smoothing the bathymetry do indeed show improved distributions of EKE (A. Semtner, personal communication, 1993).

In modeled lateral boundary layers the no-slip condition and "staircase" numerical representation of coastal boundaries contribute to noticeably lower energy in coastal boundary currents than is observed. Outside the coastal boundary layer, the region of active eddy generation where the EAC separates from the coast has EKE values typically one fourth of those observed, but this ratio drops rapidly to one eighth in the central Tasman Sea. Model animations [*Isakari et al.*, 1992] show EAC eddies do not exhibit the observed tendency to drift offshore and are dissipated too rapidly by either too strong lateral mixing or surface buoyancy flux, or both.

While differences in eddy energy reveal some systematic deficiencies of the model, the qualitative distribution of Southern Ocean eddy variability is modeled successfully. So too is the pattern of eddy momentum flux, as indicated by the coincidence in observed and modeled patterns of velocity variance ellipses. Coherent patterns in the anisotropy of velocity variance ellipses occur in regions of strong shear in the mean currents (e.g., the EAC separation and the ACC near 150°E), indicating significant interaction between the mean currents and the eddies. It is therefore reasonable to expect that the model should capture many of the essential qualitative features of eddy-mean flow interaction, even if the simulated eddy variability is too low in magnitude.

The calculation of eddy-mean interaction terms from the combination of hydrography climatology and Geosat eddy statistics is fraught with likely sources of error. The resolution of the gridded climatology is inadequate for capturing the sharp gradients in surface mean currents and is compiled from data gathered over a time period different from that of the Geosat mission. Nevertheless, the apparent agreement between modeled eddy-mean interaction terms and those estimated from data is encouraging. Though the magnitude of the conversion terms in the data and model are comparable, it is likely both underestimate the true magnitude. The modeled eddy variability should be at least fourfold greater, and since the shear in model mean currents is also likely to be limited by model resolution, the eddy-mean interaction terms could be underestimated by well in excess of the factor of 4.

In isolated regions such as the Agulhas Current, eddy momentum flux divergence and eddy-mean kinetic energy conversion are comparable in magnitude to the effects of direct wind forcing, although integrated over the entire Southern Ocean, their contribution is small. However, a fourfold increase would make the contribution of horizontal eddy transports of momentum significant, as it is in high-resolution quasi-geostrophic models. Future high-resolution primitive equation Southern Ocean simulations, or well-resolved mean currents from an altimeter, would help resolve this issue.

Appendix

Local exchanges of kinetic energy and momentum between the mean and eddy components of a flow governed by the primitive equations are determined by the following diagnostics:

Kinetic Energy Conversion

The horizontal momentum equations of the primitive equations may be written

$$u_t + uu_x + vu_y + wu_z - fv = R^u \quad (1a)$$

$$v_t + uv_x + vv_y + wv_z + fu = R^v \quad (1b)$$

where the pressure gradient and dissipation terms are represented schematically as R^u and R^v. All other notation is standard.

Variables are separated into mean and eddy parts, e.g., $u = \overline{u} + u'$, where the overbar denotes a time mean and the prime denotes the departure from this mean. Taking the time average of u' times (equation (1a)) plus v' times (equation (1b)) yields an equation for the material derivative of the eddy kinetic energy

$$\frac{D}{Dt}\tfrac{1}{2}(\overline{u'^2} + \overline{v'^2}) = \left[\overline{u'R^{u'}} + \overline{v'R^{v'}}\right] -$$

$$\left[\overline{u'u'}\,\overline{u}_x + \overline{v'u'}\,\overline{v}_x + \overline{u'v'}\,\overline{u}_y + \overline{v'v'}\,\overline{v}_y + \overline{u'w'}\,\overline{u}_z + \overline{v'w'}\,\overline{v}_z\right] \quad (2)$$

Similarly, the time average of $\overline{u}$ times (equation (1a)) plus $\overline{v}$ times (equation (1b)) yields a mean kinetic energy equation

$$\frac{D}{Dt}\tfrac{1}{2}(\overline{u}^2 + \overline{v}^2) = \left[\overline{uR^u} + \overline{vR^v}\right] - \left[(\overline{u}\,\overline{u'u'})_x + (\overline{u}\,\overline{v'u'})_y + \right.$$

$$\left.(\overline{u}\,\overline{w'u'})_z + (\overline{v}\,\overline{u'v'})_x + (\overline{v}\,\overline{v'v'})_y + (\overline{v}\,\overline{w'v'})_z\right] +$$

$$\left[\overline{u'u'}\,\overline{u}_x + \overline{v'u'}\,\overline{v}_x + \overline{u'v'}\,\overline{u}_y + \overline{v'v'}\,\overline{v}_y + \overline{u'w'}\,\overline{u}_z + \overline{v'w'}\,\overline{v}_z\right] \quad (3)$$

The final term in brackets in (3) is the same term but with opposite sign to that in (2). It represents exchange of kinetic energy between the eddies and the mean flow. The contribution to this term from the vertical Reynolds stress $(\overline{u'w'}, \overline{v'w'})$ cannot be estimated from altimeter data but will be neglected because vertical velocity perturbations are weak near the sea surface. Therefore when the term

$$\overline{u'u'}\overline{u}_x + \overline{v'u'}\overline{v}_x + \overline{u'v'}\overline{u}_y + \overline{v'v'}\overline{v}_y \qquad (4)$$

is positive (negative), this implies transfer of kinetic energy to (from) the mean flow from (to) the eddies.

Eddy Momentum Flux Divergence

Denoting the local horizontal mean current $(\overline{u}, \overline{v})$ by the vector $\overline{\mathbf{u}}$, a unit vector e parallel to the mean flow may be defined as $\mathbf{e} = (e_u, e_v) = (\overline{u}, \overline{v})/|\overline{\mathbf{u}}|$. Then the momentum balance in local alongstream coordinates is obtained from the vector product of e and the time average of (1)

$$\frac{D}{Dt}|\overline{\mathbf{u}}| = \frac{1}{|\overline{\mathbf{u}}|}\left[\overline{u}(R^{\overline{u}} + f\overline{v}) + \overline{v}(R^{\overline{v}} - f\overline{u})\right] -$$

$$\frac{1}{|\overline{\mathbf{u}}|}\left[\overline{u}(\overline{u'u'_x} + \overline{v'u'_y} + \overline{w'u'_z}) + \overline{v}(\overline{u'v'_x} + \overline{v'v'_y} + \overline{w'v'_z})\right] \qquad (5)$$

Using continuity to rewrite the Reynolds stress components and again neglecting the contribution of the vertical velocity perturbations, the final term in brackets may be written

$$-\frac{1}{|\overline{\mathbf{u}}|}\left[\overline{u}(\overline{u'u'}_x + \overline{v'u'}_y) + \overline{v}(\overline{u'v'}_x + \overline{v'v'}_y)\right] \qquad (6)$$

When this term is positive (negative), it implies eddy momentum flux divergence transfers momentum to (from) the mean flow from (to) the eddies.

Acknowledgments. This work contributes to the CSIRO Climate Change Research Program. JLW is funded by Australia's National Greenhouse Research Program. RAM was supported by an Australian Post-Graduate Research Award and a CSIRO Post-Graduate Scholarship. We thank A. Semtner and R. Chervin for generously making available the results of stage 5 of their model run in advance of publication and for providing support for model analysis at the National Center for Atmospheric Research. NCAR is funded by the National Science Foundation.

References

Böning, C. W., and R. G. Budich, Eddy dynamics in a primitive equation model: Sensitivity to horizontal resolution and friction, *J. Phys. Oceanogr.*, *22*, 361–381, 1992.

Böning, C. W., R. Döscher, and R. G. Budich, Seasonal transport variation in the western subtropical North Atlantic: Experiments with an eddy-resolving model, *J. Phys. Oceanogr.*, *21*, 1271–1289, 1991.

Bryan, F. O., and W. R. Holland, A high resolution simulation of the wind- and thermohaline-driven circulation in the North Atlantic Ocean, in *Parameterization of Small-Scale Processes*, edited by P. Muller, and D. Henderson, pp. 99–116, 'Aha Huliko'a Winter Workshop, Honolulu, Hawaii, 1989.

Bryden, H. L., The Southern Ocean, in *Eddies in Marine Science*, edited by A. Robinson, pp. 265–277, Springer-Verlag, New York, 1983.

Bryden, H. L., and R. A. Heath, Energetic eddies at the northern edge of the Antarctic Circumpolar Current in the south west Pacific, *Prog. Oceanogr.*, *14*, 65–87, 1985.

Emery, W. J., W. G. Lee, and L. Magaard, Geographic and seasonal distributions of Brünt-Väisälä frequency and Rossby radii in the North Pacific and North Atlantic, *J. Phys. Oceanogr.*, *14*, 294–317, 1984.

Fine Resolution Antarctic Model (FRAM) Group (D. Webb and others), An eddy-resolving model of the Southern Ocean, *Eos Trans. AGU*, *72*(15), 169–175, 1991.

Gordon, A. L., and E. Molinelli, *Southern Ocean Atlas*, Columbia University Press, New York, 1982.

Houry, S., E. Dombrowsky, P. De Mey, and J.-F. Minster, Brünt-Väisälä frequency and Rossby radii in the South Atlantic, *J. Phys. Oceanogr.*, *17*, 1619–1626, 1987.

Inoue, M., Modal decomposition of the low-frequency currents and baroclinic instability at Drake Passage, *J. Phys. Oceanogr.*, *15*, 1157–1181, 1985.

Isakari, S., M. P. McCann, and A. J. Semtner, Jr., A video atlas of global ocean circulation, Alpine Productions, Naval Postgraduate School, Monterey, Calif., 1992.

Johnson, G. C., and H. L. Bryden, On the size of the Antarctic Circumpolar Current, *Deep Sea Res.*, *36*, 39–53, 1989.

Luyten, J. A., A. Spencer, S. Tarbell, K. Luetkemeyer, P. Flament, J. Toole, M. Francis, and S. Bennett, Moored current meter, AVHRR, CTD, and drifter data from the Agulhas current retroflection region (1985–1987) Vol. XLII, Woods Hole Oceanogr. Inst. Tech. Rep. WHOI-90-30, Woods Hole, Mass., 1990.

McWilliams, J. C., W. R. Holland, and J. H. S. Chow, A description of numerical Antarctic Circumpolar Currents, *Dyn. Atmos. Oceans*, *2*, 213–291, 1978.

Morrow, R. A., J. A. Church, R. Coleman, D. Chelton, and N. White, Eddy momentum flux and its contribution to the Southern Ocean momentum balance, *Nature*, *357*, 482–484, 1992.

Morrow, R. A., R. Coleman, J. A. Church, and D. B. Chelton, Surface eddy momentum flux and velocity variance in the Southern Ocean from Geosat altimetry, *J. Phys. Oceanogr.*, 1994, submitted.

Mulhearn, P. J., The Tasman front: A study using satellite infrared imagery, *J. Phys. Oceanogr.*, *17*, 1148–1155, 1987.

Patterson, S. L., Surface circulation and kinetic energy distributions in the southern hemisphere oceans from FGGE drifting buoys, *J. Phys. Oceanogr.*, *15*, 865–884, 1985.

Semtner, A. J., Jr., and R. M. Chervin, A simulation of the global ocean circulation with resolved eddies, *J. Geophys. Res.*, *93*, 15502–15522, 1988.

Semtner, A. J., Jr., and R. M. Chervin, Ocean general circulation from a global eddy-resolving model, *J. Geophys. Res.*, *97*, 5493–5550, 1992.

Spall, M. A., Circulation in the Canary Basin: A model/data analysis, *J. Geophys. Res.*, *95*, 9611–9628, 1990.

Stammer, D., and C. W. Böning, Mesoscale variability in

the Atlantic Ocean from GEOSAT altimetry and WOCE high resolution numerical modelling, *J. Phys. Oceanogr.*, *22*, 732–752, 1992.

Treguier, A. M., Kinetic energy analysis of an eddy resolving, primitive equation model of the North Atlantic, *J. Geophys. Res.*, *97*, 687–701, 1992.

Wolff, J.-O., E. Maier-Reimer, and D. J. Olbers, Wind-driven flow over topography in a zonal β-plane channel: A quasi-geostrophic model of the Antarctic Circumpolar Current, *J. Phys. Oceanogr.*, *21*, 236–264, 1991.

R. A. Morrow, UMR39/GRGS, 18 av. E. Belin, 31055 Toulouse, France. e-mail: morrow@thor.cnes.fr.

J. L. Wilkin, CSIRO Division of Oceanography, GPO Box 1538, Hobart, Tasmania 7001, Australia. e-mail: wilkin@flood.ml.csiro.au.

(Received June 21, 1993; revised September 13, 1993; accepted October 29, 1993.)